IL NUOVO CIMENTO Vol. 24 C, N. 4-5 Luglio-Ottobre 2001

Hadron-hadron and hadron-nuclei collisions at high energies(*)

G. Giacomelli and R. Giacomelli

Dipartimento di Fisica dell'Università di Bologna e INFN - I-40127 Bologna, Italy

(ricevuto il 28 Ottobre 2000; approvato il 12 Febbraio 2001)

Summary. — A brief review is made of the present situation of hadron-hadron and hadron-nuclei total elastic and inelastic cross-sections at high energies.

PACS 13.85.Dz – Elastic scattering.
PACS 13.85.Fb – Inelastic scattering: two-particle final states.
PACS 13.85.Hd – Inelastic scattering: many-particle final states.
PACS 01.30.Cc – Conference proceedings.

1. – Introduction

In the 1960's-1980's high-quality secondary beams became available at proton synchrotrons of increasing energies (PS, AGS, IHEP, FNAL, SPS). The secondary charged hadron beams contained the six stable or quasi stable charged particles $\pi^{\pm}$, $K^{\pm}$, p, $\overline{p}$. The main experimental lines of research were: i) total hadron-hadron (hh) cross-section measurements at high energies ($p_{lab} > 20$ GeV/c); ii) elastic hh scattering measurements; iii) measurements of absorption cross-sections of hadrons in nuclei (as byproducts of hh total cross-section measurements); iv) hadron production at forward angles in p-nuclei collisions, and v) inelastic hh collisions [1-5]. In some high-intensity beams many particle searches were made, which also lead to the study of $\overline{d}$, $\overline{t}$ and $\overline{He_3}$ production [6].

In order to reach higher energies it became necessary to build hadron colliders. The first was the ISR pp and $p\overline{p}$ collider at CERN, which allowed to reach c.m. energies between 22 and 63 GeV; then the $Sp\overline{p}S$ collider at CERN allowed $p\overline{p}$ collisions from 600 to 900 GeV; finally the Fermilab Tevatron collider allowed $p\overline{p}$ collisions up to 1.8 TeV.

The first experiments performed at the ISR were relatively simple dedicated experiments, like those for total cross-section and elastic scattering measurements, and single arm spectrometers for the study of inelastic collisions [7, 8]. Then followed general purpose detectors: the SFM at the ISR [9], the general purpose detectors UA1 and UA2 and

(*) Paper presented at the Chacaltaya Meeting on Cosmic Ray Physics, La Paz, Bolivia, July 23-27, 2000.

experiment UA4 at the Sp$\overline{\text{p}}$S collider, and finally the general purpose detectors CDF, D0 and the specialized experiments E710, F8 at Fermilab [10].

The highest energies were and are still obtainable only with cosmic rays. We shall discuss total cross-sections at high energies, the high energy low-p_{t} parameters and some features of inelastic collisions [11, 12].

2. – Hadron-hadron total cross-sections

At fixed target accelerators (AGS, IHEP, FNAL) the total cross-sections were measured with the transmission method, with relative precisions smaller than 1% and systematic scale errors of about 2%. The measurements of the total cross-sections at the pp and $\overline{\text{p}}$p colliders required the development of new experimental techniques: the scattering of particles was measured at very small angles, with detectors positioned in re-entrant containers ("Roman pots") located very close to the circulating beams. The combinations of statistical and systematic uncertainties are $\geq 10\%$. Figure 1 summarizes the present status of high energy total cross-section measurements: for $E_{\text{cm}} = \sqrt{s} > 3.4$ GeV all total hh cross-sections decrease, reach a minimum and then increase with increasing energy (the K^+p total cross-section was already increasing at Serpukhov energies [1]). Moreover the differences between the cross-sections $\overline{\text{x}}$p and xp decrease with increasing energy [5].

There is not a unique interpretation for this rise, though in many QCD-inspired models it seems to be connected with the increase of the number of minijets and thus to semi-hard gluon interactions.

Most of the high energy elastic and total cross-section data have been usually interpreted in terms of Regge Poles, and thus in terms of Pomeron exchange. Even if the Pomeron was introduced long time ago we do not have a consensus on its exact definition and on its detailed substructure. Some authors view it as a "gluon ladder".

Future experiments on hadron-hadron total cross-sections remain centered at the Fermilab Collider (for p$\overline{\text{p}}$). The near future will rely on the BNL-RICH Collider, and later, on the LHC proton-proton and heavy-ion Collider at CERN. Large-area cosmic ray experiments may be able to improve the data in the ultrahigh energy region [12].

3. – Hadron-hadron elastic scattering

The differential cross-section for the elastic scattering of unpolarized particles from unpolarized targets has a simple structure in the high energy region. It depends on two variables: the energy and an angular variable, which is usually chosen to be the square of the four momentum transfer t. The energy dependence is of the $\ln\ s$ type. The angular distribution may be divided in four regions: i) the Coulomb region for $|t| < 0.001$ $(\text{GeV/c})^2$; ii) the Coulomb-nuclear interference region for $0.001 < |t| < 0.01$ $(\text{GeV/c})^2$; measurements in this region yield information on the ratio ρ of the real to the imaginary part of the forward scattering amplitude; iii) the nuclear diffraction region proper for $0.01 < |t| < 0.5$ $(\text{GeV/c})^2$; here the most important parameter is the slope B, or the slopes b_i, of the diffraction pattern; iv) the large angle region for $|t| > 0.5$ $(\text{GeV/c})^2$: for $E_{\text{cm}} \leq 100$ GeV it is characterized by a dip-bump structure which resembles that from diffraction from an opaque disc. Most of these features are observed in the pp and $\overline{\text{p}}$p elastic scattering angular distributions at $E_{\text{cm}} = 53$, 546 and 1400 GeV, see fig. 2.

One usually defines the following high energy scattering parameters: i) the total cross-section, σ_{t}; ii) the slope B of the differential elastic nuclear cross-section $\text{d}\sigma/\text{d}t = Ae^{Bt}$,

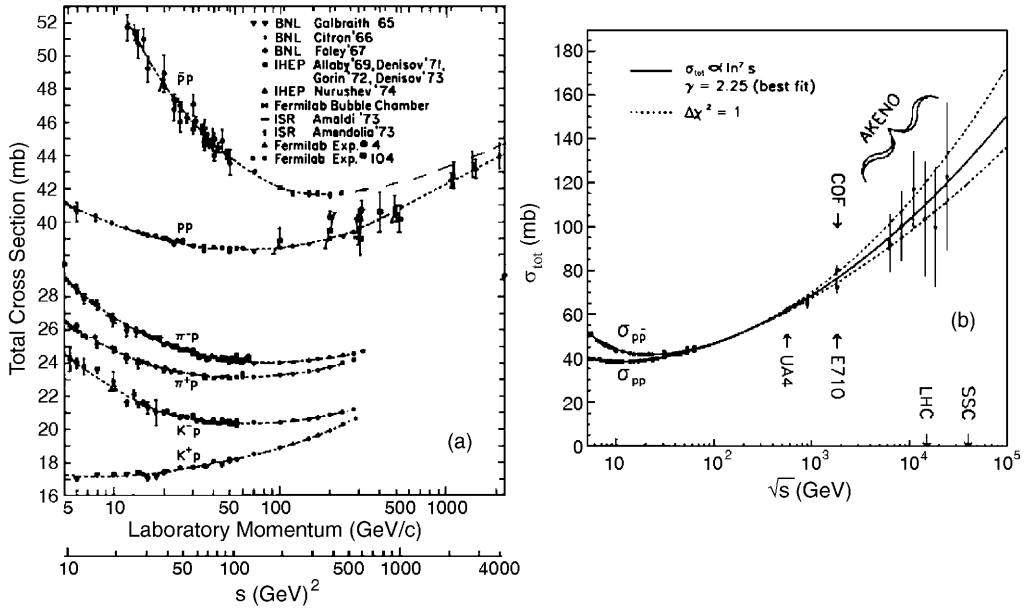

Fig. 1. – Compilation of total cross-sections (a) for high-energy hh scattering and (b) for higher energy $\overline{\mathrm{p}}\mathrm{p}$ and pp, including cosmic ray measurements; the solid line is a fit; the uncertainty region is delimited by dashed lines.

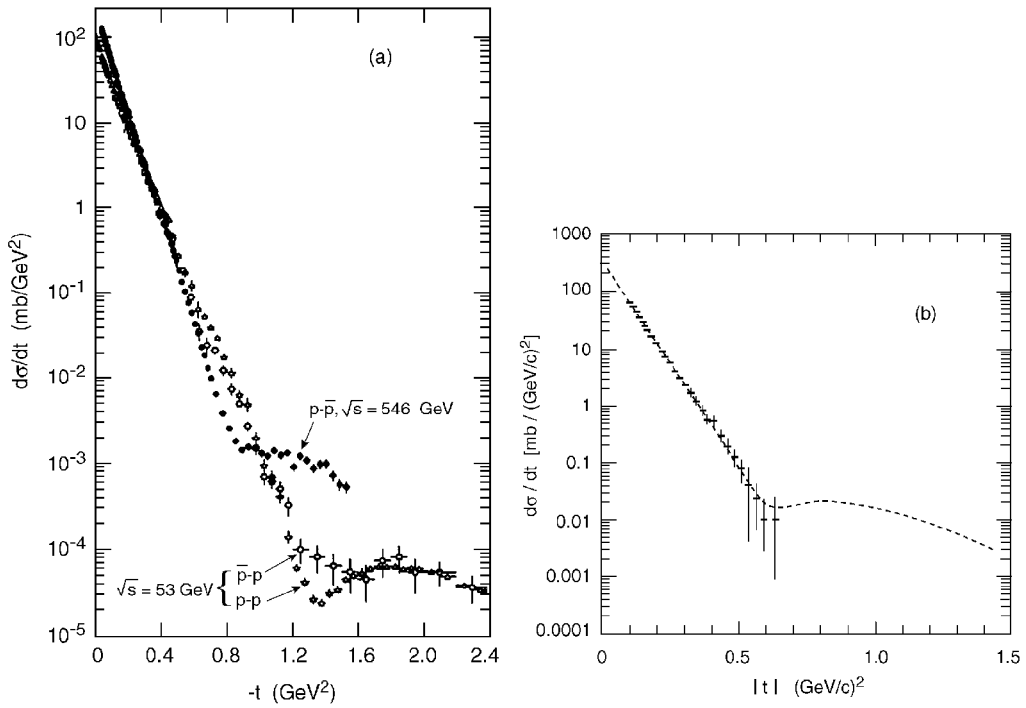

Fig. 2. – Differential elastic cross-sections for pp and $\overline{\mathrm{p}}\mathrm{p}$ (a) at 53 and 546 GeV, (b) at 1.8 TeV.

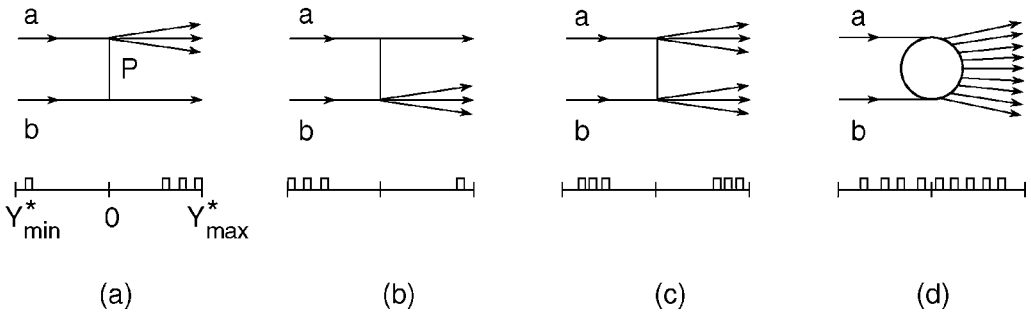

Fig. 3. – Pictorial description of inelastic, small p_{t} processes with characteristic rapidity distributions. P indicates Pomeron exchange. (a) Fragmentation of the beam particle a; (b) fragmentation of the target b; (c) double fragmentation of a and b; (d) central collision.

at $|t| \simeq 0.1$ (GeV/c)^2; iii) the ratio $\rho = (\mathrm{Re}\, A/\mathrm{Im}\, A)_{t=0}$; iv) the opacity $O = 2\sigma_{\mathrm{el}}/\sigma_{\mathrm{t}}$. At very high energies σ_{t}, B and O rise with energy, while ρ is slightly positive. From the behaviour of these parameters there emerges the picture of a proton which becomes bigger (larger B) and more opaque (larger O) as the energy increases. At the highest energy $O \simeq 0.48$, which is still smaller than the black disk value of 1.

4. – Hadron-hadron inelastic processes

Figure 3 shows pictorially various inelastic processes at low-p_{t}: single and double diffraction dissociation and inelastic processes; these are the dominant processes with the largest cross-sections, concentrated in particular in the very forward angular region: this is the region which is most important for cosmic ray experiments.

At high energies the total $\overline{\mathrm{p}}\mathrm{p}$ cross-section may be written as

$$\sigma_{\mathrm{t}} = \sigma_{\mathrm{el}} + \sigma_{\mathrm{inel}} = \sigma_{\mathrm{el}} + \sigma_{\mathrm{sd}} + \overline{\sigma}_{\mathrm{sd}} + \sigma_{\mathrm{dd}} + \sigma_{\mathrm{nd}}\,, \tag{1}$$

where σ_{el} is the elastic cross-section, σ_{sd} is the single diffractive cross-section when the incoming proton fragments into a number of particles, $\overline{\sigma}_{\mathrm{sd}}$ is the single diffractive cross-section for the fragmentation of the antiproton (at high energies $\sigma_{\mathrm{sd}} = \overline{\sigma}_{\mathrm{sd}}$). σ_{dd} is the double diffractive cross-section, σ_{nd} is the non-diffractive part of the inelastic cross-section (fig. 3). The elastic, single diffractive and double diffractive processes give rise to low multiplicity events with particles emitted in the very forward region in the c.m. system. The non-diffractive cross-section is the main part of the inelastic cross-section; it gives rise to high multipliciy events and to particles emitted at all angles. Most of the non-diffractive cross-section concerns particles emitted with low transverse momentum (*low-p_{t} physics*) with properties which change slowly with c.m. energy ($\ln s$ *physics).* A small part of the non-diffractive cross-section is due to central collisions among the colliding particles and gives rise to high p_{t} jets of particles emitted at relatively large angles (*large p_{t} physics).* The contribution of jet physics increases with c.m. energy.

In fig. 4a, the average charged multiplicities in pp and $\overline{\mathrm{p}}\mathrm{p}$ collisions are shown *vs.* $\sqrt{s}$. The data may be fitted to a power law of $\ln\ s$:

$$\overline{\mathrm{n}} = A + B\ \ln\ s + C\ \ln^2\ s \simeq 3.6 - 0.45\ \ln\ s + 0.20\ \ln^2\ s\,. \tag{2}$$

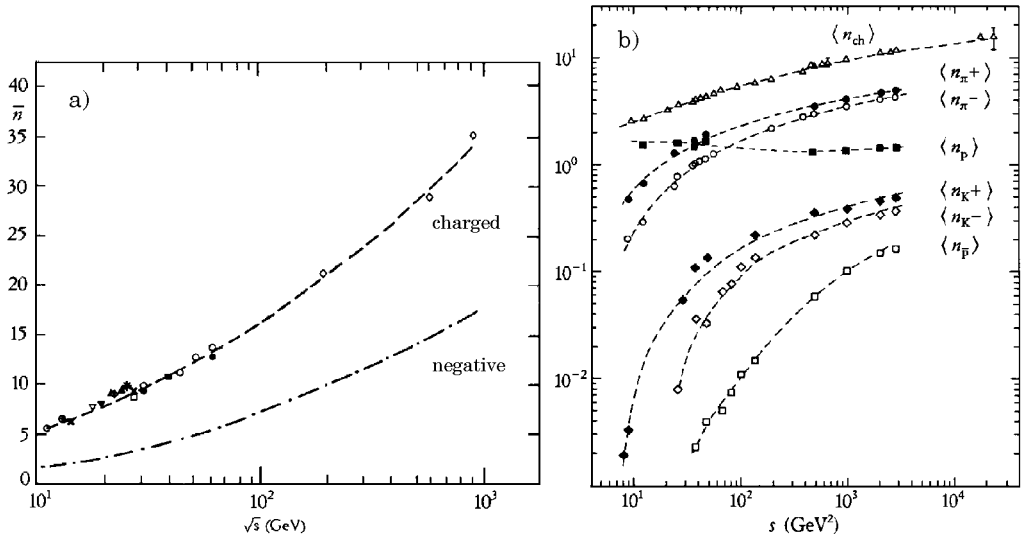

Fig. 4. – (a) Average charged multiplicities $\overline{n}$ for pp and $\overline{p}p$ collisions *vs.* $E_{cm} = \sqrt{s}$. (b) Average number of $\pi^{\pm}$ $K^{\pm}$, p and $\overline{p}$ produced in pp collisions up to $E_{cm} = 63$ GeV.

At $\sqrt{s} = 1.8$ TeV are produced on average 40 charged and 20 neutral particles. Figure 4b shows the average number of $\pi^{\pm}$, $K^{\pm}$, p and $\overline{p}$ produced in pp collisions up to $\sqrt{s} \simeq 100$ GeV. Pions are the dominantly produced hadrons. Hadrons are mainly produced at low transverse momenta. The average p_t increases slowly with $\sqrt{s}$: it is $\langle p_t \rangle \simeq 0.36$ GeV/c in $20 < \sqrt{s} < 100$ GeV; then it increases slowly up to $\simeq 0.46$ GeV/c at $\sqrt{s} = 1.8$ TeV. The simplest interpretation of these features is in terms of thermodynamic models: hadrons are emitted from a region with a temperature $T \simeq 130$–200 MeV. QCD, at present, cannot be used to calculate the data at low p_t, because the strong coupling constant is large and perturbative methods cannot be used. Therefore one has to use models. Hard collisions can instead be calculated by perturbative QCD.

5. – Hadron-nucleus and nucleus-nucleus collisions

Usually, as byproducts of hh total cross-section measurements, the absorption cross-sections of $\pi^{\pm}$, $K^{\pm}$, p and $\overline{p}$ on various nuclei (Li, C, Al, Cu, Sn, and Pb) were measured at incident lab momenta up to 280 GeV/c [2, 4, 11]. Most absorption cross-sections decrease slowly for p_{lab} up to $\simeq 50$ GeV/c; for higher p_{lab} they are almost constant.

The data at each energy were fitted to the simple expression

$$\sigma_a(A) = \sigma_0 A^{\alpha}\,, \tag{3}$$

where A is the atomic weight of the target nucleus. Examples are shown in fig. 5a at three lab momenta for three different incoming hadrons. For all incident particles except antiprotons, the value of σ_0 increases by up to 10% as the incident p_{lab} increases from 60 to 280 GeV/c, with the largest increase for K^+. For $\overline{p}$, σ_0 decreases with increasing p_{lab}. Figure 5b shows the parameters σ_0 and α *vs.* the corresponding hp total cross-section: σ_0 rises monotonically with σ_{hp}; the values of α are consistent with α approaching 0.67 for large values of σ_{hp} as would be expected for an opaque nucleus.

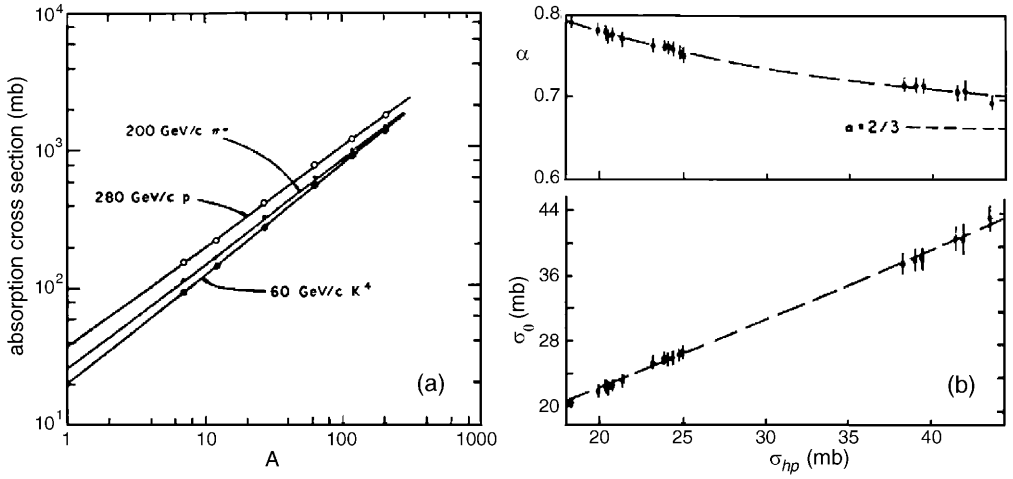

Fig. 5. – (a) Absorption cross-sections *vs.* atomic weight; the solid lines are fits to eq. (3). (b) The parameters σ_0 and α *vs.* the corresponding hp total cross-sections, $\sigma_{\rm hp}$.

The fragmentation cross-sections of various nuclei were measured at many energies using nuclear track detectors, which yield high-resolution measurements of the restricted energy loss. This arises from the relatively low energy required to break the polymeric bonds of the detectors and because fluctuations due to energetic δ-electrons do not contribute to the latent track formation. The radiation damage along the path of an incoming nucleus may be developed to microscope-visible cones by chemical etching. Figure 6a shows the charge distribution obtained with 200 GeV/nucleon S^{16+} ions and their fragments produced in a Cu target [13]: notice the good charge resolution and the absence of nuclei with fractional charges. The cross-sections in fig. 6b are relative to fragments of 158 GeV/nucleon Pb^{82+} ions in a target with $\overline{A} = 11.5$ with a variation of atomic number $\Delta Z = 1$–7 with respect to the $Z = 82$ of the incoming ions.

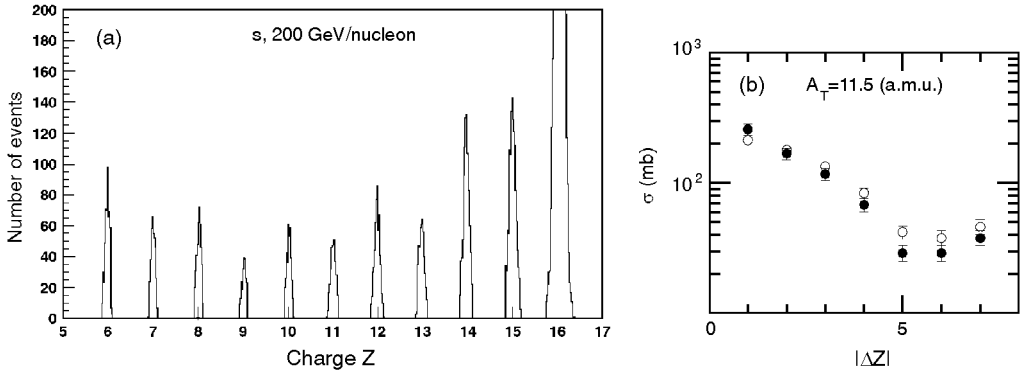

Fig. 6. – (a) Charge distribution of 200 GeV/nucleon S^{16+} ions and their fragments [13]. (b) Cross-sections in a target $\overline{A} = 11.5$ of 168 GeV/nucleon Pb^{82+} ions into nuclear fragments for ΔZ ranging from 1 to 7; the open and black points refer to two different computing methods.

6. – Conclusions. Perspectives

A wealth of experimental information has been obtained since the early 1960's on high-energy hadron-hadron and hadron-nucleus cross-sections, starting with simple equipments and proceeding to more complex apparata and better beams.

The higher energy data coming from collider experiments have large systematic uncertainties, mainly connected to the poor knowledge of the collider luminosity, the difficulty of measuring with some precision the single and double diffraction cross-sections, etc.

Most of the information on hadron-hadron collisions was interpreted in terms of phenomenological models. Much more work is needed to interpret and systemize the available data, since only the small part of the cross-section corresponding to large transverse momenta may be interpreted in terms of QCD.

Few and not too precise data are available at very low p_{t} and very small angles, which is the region where more interest lies for cosmic rays. The information is here codified in Monte Carlos, which are becoming progressively more complicated. The Monte Carlos include hadron-nucleus collisions (for which the data are much less abundant than for hh collisions); hadron-nucleus effects are mainly interpreted in the context of the Gluber model [14].

Nucleus-nucleus data are even less abundant, and the Monte Carlos have extra complications coming from the used models [14].

In the near future the RICH collider at BNL should provide data on nucleus-nucleus collisions. In the future the different experiments at the LHC collider should provide data on hh, hadron-nuclei and nuclei-nuclei collisions at much higher energies.

* * *

We thank many colleagues for their collaboration, for many discussions and for explanations of Cosmic Ray Monte Carlos. We thank Ms L. De Angelis for typing the manuscript.

REFERENCES

[1] Allaby J. V. *et al.*, *Phys. Lett. B*, **30** (1969) 500; Denisov S. P. *et al.*, *Phys. Lett. B*, **36** (1971) 415; *Yad Fis*, **14** (1971) 998.
[2] Binon F. *et al.*, *Phys. Lett. B*, **31** (1970) 230.
[3] Baker W. F. *et al.*, *Nucl. Phys. B*, **51** (1974) 303; Carroll A. S. *et al.*, *Phys. Rev. Lett.*, **33** (1974) 928; 932; *Phys. Lett. B*, **61** (1976) 303; **80** (1979) 423.
[4] Carroll A. S. *et al.*, *Phys. Lett. B*, **80** (1979) 319.
[5] Giacomelli G., *Prog. Nucl. Phys.*, **12** (1970) 77.
[6] Bozzoli W. *et al.*, *Nucl. Phys. B*, **140** (1978) 271; **144** (1978) 317; **159** (1979) 363; Bussiere A. *et al.*, *Nucl. Phys. B*, **174** (1980) 1.
[7] Amaldi U. *et al.*, *Phys. Lett. B*, **44** (1973) 112; Amendolia S. R. *et al.*, *Phys. Lett. B*, **44** (1973) 119; Carboni G. *et al.*, *Nucl. Phys. B*, **254** (1985) 69; Giacomelli G. and Jacob M., *Phys. Rep.*, **55** (1979) 1.
[8] Bertin A. *et al.*, *Phys. Lett. B*, **38** (1972) 260; **42** (1972) 493; Antinucci M. *et al.*, *Nuovo Cimento Lett.*, **6** (1973) 121; Capiluppi P. *et al.*, *Nucl. Phys. B*, **70** (1974) 1; **79** (1974) 189; Albini E. *et al.*, *Nuovo Cimento*, **32** (1976) 101.
[9] Breakstone A. *et al.*, *Phys. Lett. B*, **132** (1983) 458; *Nucl. Phys. B*, **248** (1984) 253; *Phys. Rev. Lett.*, **54** (1985) 2180.
[10] Amos N. A. *et al.*, *Phys. Rev. Lett.*, **63** (1989) 2784; *Phys. Lett. B*, **247** (1990) 127; **243** (1990) 158.

[11] Baker W. F. *et al.*, (Production of $\pi^{\pm}$, $K^{\pm}$, p and $\overline{p}$ by 400 GeV/c protons) Fermilab-78/79-EXP (1978).
[12] Giacomelli G., *Int. J. Mod. Phys. A*, **5** (1990) 223; *Hadron-hadron and hadron-nuclei interactions at intermediate and high energies 1994 Marshak Memorial*, DFUB 9/94 (1994); *Total cross-sections, Kycia Memorial Symposium*, 19/5/2000, BNL, hep-ex/0006038; *Prog. Nucl. Phys.*, **12** (1970) 77.
[13] Cecchini S. *et al.*, *Astropart. Phys.*, **1** (1993) 369; Giacomelli G. *et al.*, *Nucl. Instrum. Methods A*, **411** (1998) 41; Dekhissi H. *et al.*, *Nucl. Phys. A*, **662** (2000) 207.
[14] Capella A. *et al.*, *Phys. Rep.* , **2** (3) 6 (1994); Glauber J. J. *et al.*, *Nucl. Phys. B*, **21** (1970) 135; Ranft J., *Phys. Rev. D*, **51** (1995) 64.